Molecular Cell, *Volume 40*

Supplemental Information

3D Cryo-EM Structure of an Active Step I Spliceosome and Localization of Its Catalytic Core

Monika M. Golas, Bjoern Sander, Sergey Bessonov, Michael Grote, Elmar Wolf, Berthold Kastner, Holger Stark, and Reinhard Lührmann

This Supplemental Information contains:

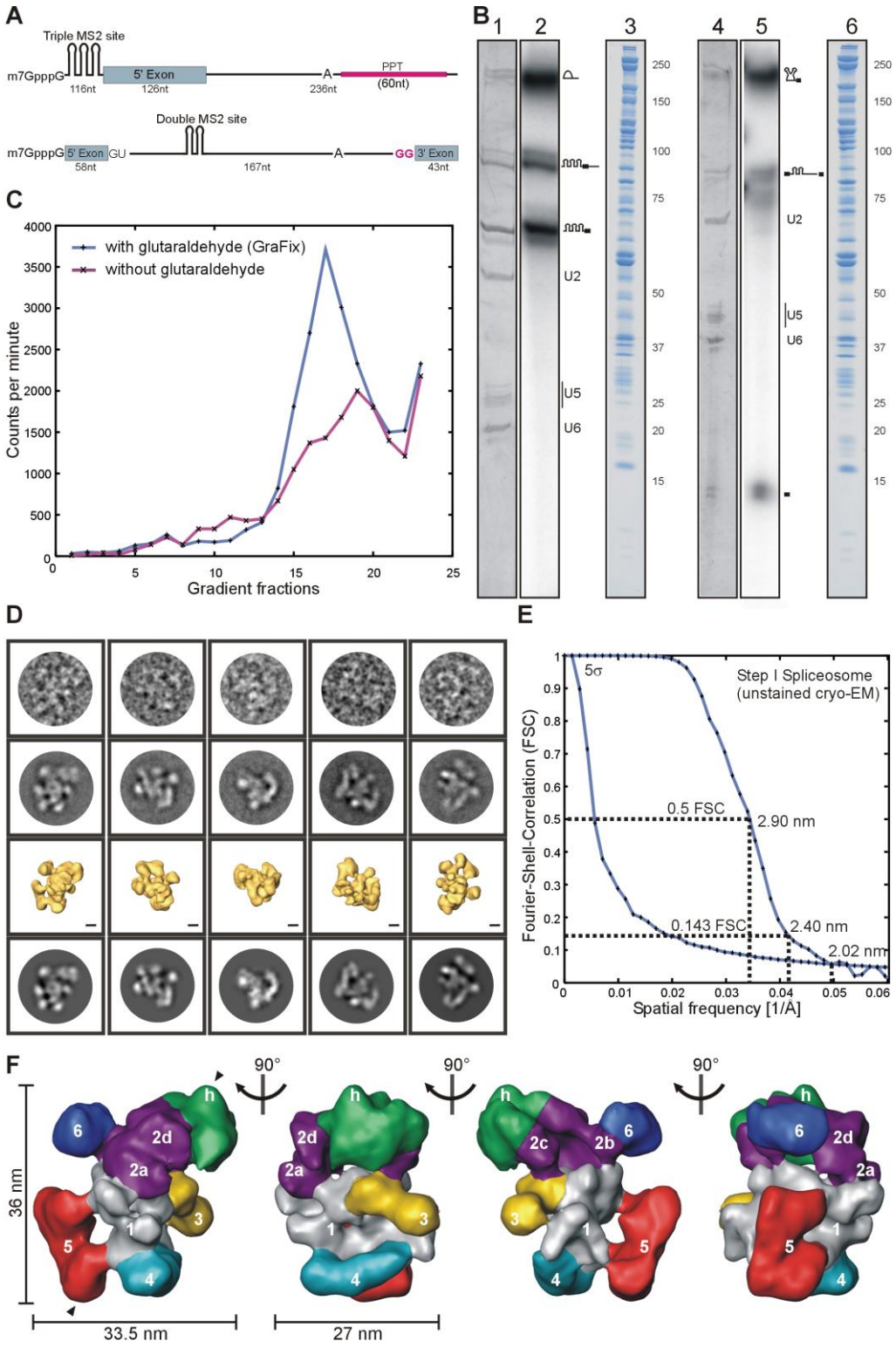

Figure S1. Human Spliceosomal C Complexes Assembled on the PM5 or MINX$_{GG}$ Construct, Related to Figure 2

A. Schematic representation of the PM5 (top) and MINX$_{GG}$ (bottom) pre-mRNA constructs. **B.** RNA and protein composition of the step I spliceosome assembled on the

PM5 pre-mRNA (lanes 1–3) and $MINX_{GG}$ pre-mRNA construct (lanes 4–6). The RNA composition was determined by denaturing PAGE (lanes 1, 2, 4, 5) and the protein composition by SDS-PAGE (lane 3 and 6). RNA was visualized by silver staining (lane 1 and 4) or by autoradiography (lane 2 and 5), and protein by staining with Coomassie blue (lane 3 and 6). Identities of RNAs (lanes 1, 2, 4 and 5) and the molecular weight marker (lane 3 and 6; in kDa) are indicated on the right, respectively. **C.** Influence of GraFix on the structural integrity of the spliceosomal complexes. Shown is the gradient profile of the final ultracentrifugation step in the absence (purple curve) or presence – i.e. GraFix (blue curve) – of a low, increasing concentration of glutaraldehyde (0–0.1%). Gradients were fractionated from the bottom (i.e. fraction #1 corresponds to the bottom fraction of the gradient). Particles purified using the GraFix protocol exhibited a sharp peak. In contrast, particles purified in a parallel gradient lacking glutaraldehyde exhibited a broader peak that was shifted somewhat to lower molecular weight fractions. Although similar amounts of step I spliceosomes were loaded onto each gradient, less overall material was observed in the gradient without glutaraldehyde while more radioactivity was found on the walls of the gradient tube. Together, this suggests dissociation and/or aggregation of the particles during ultracentrifugation in the absence of glutaraldehyde. **D.** Gallery of 5 selected particle views of the spliceosomal C complex. The upper row shows band-pass filtered images of individual particles, and the second row shows the corresponding class averages, i.e. cluster centers in an MSA-based unsupervised image clustering. Upon Euler angle determination, row 3 shows the 3D structure under the same view as the two-dimensional projection views in row 2, and row 4 shows computed re-projections from the 3D structure, which are in excellent agreement with the class averages in row 2. The scale bars correspond to 10 nm. **E.** Fourier-Shell-Correlation (FSC) analysis of the refined cryo-EM map of the step I spliceosome determined from unstained cryo-EM images. The FSC of the cryo-EM map of the step I spliceosome suggests a resolution of 2.02–2.90 nm depending on the criteria used (i.e. 5σ, 0.143 FSC, 0.5 FSC). **F.** 3D structure of the step I spliceosome assembled on the PM5 pre-mRNA. The C complex has a size of ~36 nm × 33.5 nm × 27 nm with maximum dimensions of ~42 nm (diagonal as indicated by the arrowheads). The domain numbering is as in Figure 2; densities are colored in silver, purple, green, gold, turquoise, red and blue according to the domain identity.

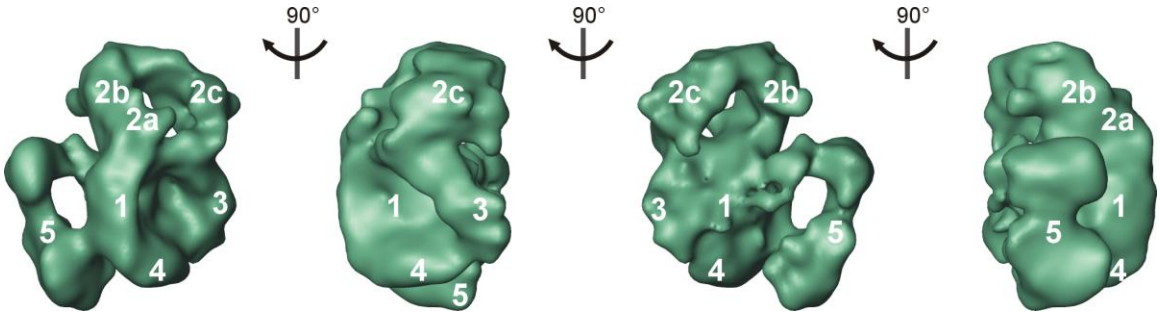

Figure S2. Three-Dimensional Structure of the Salt-stable RNP Core of the Step I Spliceosome as Determined by Weighted Averaging of Random Conical Tilt 3D maps, Related to Figure 3

Subsequent to 3D alignment and weighted integration of the 3D RCT maps over all rotations, a weighted average 3D structure of the salt-stable RNP core complex of the C complex was determined. This structure was used as reference to align the 3D RCT maps as prerequisite for 3D classification of the maps shown in Figure 3D of the main manuscript.

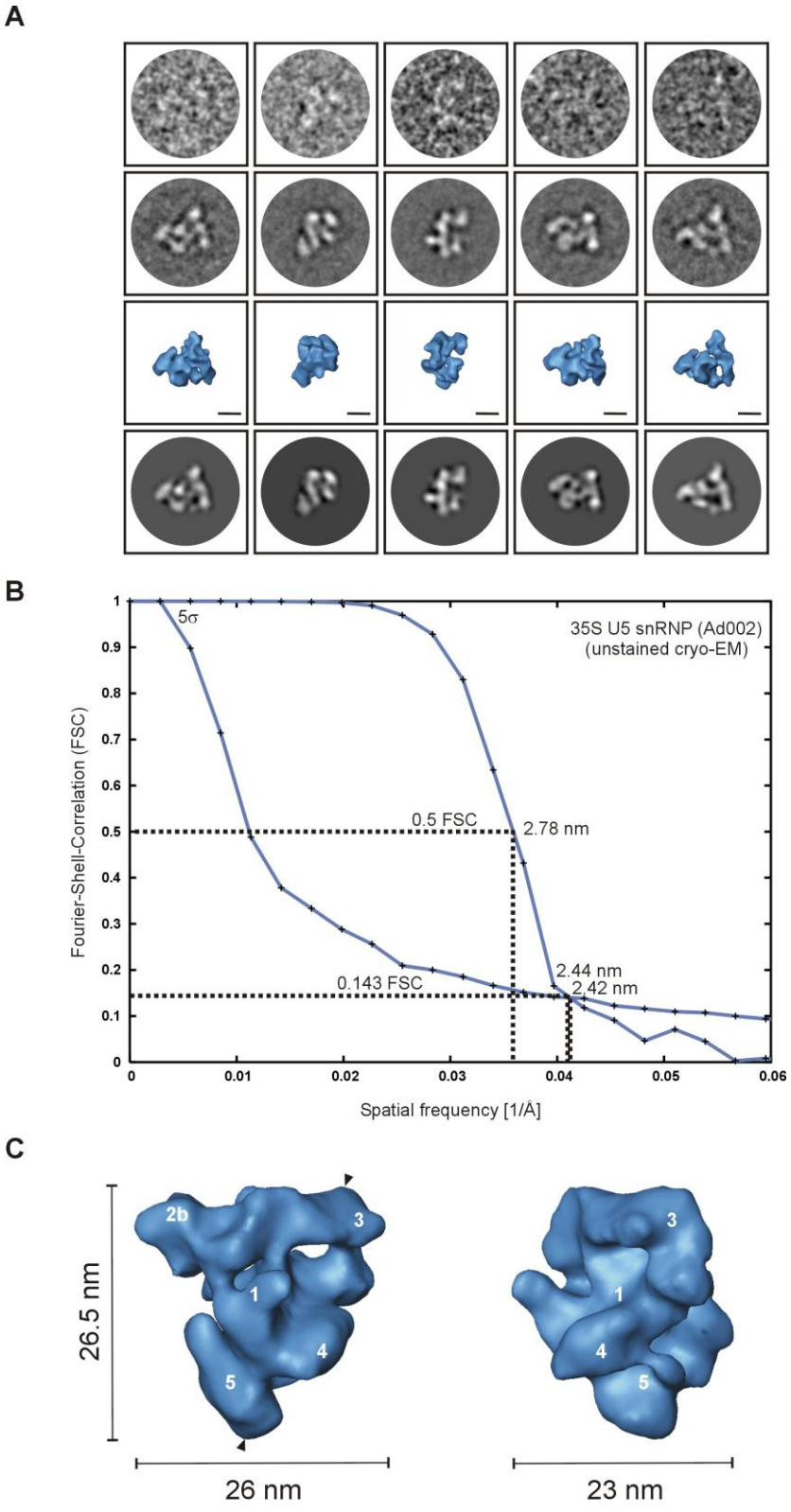

Figure S3: Three-Dimensional Structure of the 35S U5 snRNP, Related to Figure 4
35S U5 snRNPs were purified by anti-FLAG immuno-chromatography and exhibited essentially the same protein composition as found in our earlier study (Makarov et al.,

2002), except that a few proteins such as S100A8/A9, KIAA0773 and FLJ10206, which were present in substoichiometric amounts in our earlier preparations, were absent from the preparations described here (in fact, these proteins have never been observed in native spliceosomal complexes indicating that they were contaminants). On the other hand, the proteins Morg1, Q9BRR8, hPrp22 and Slu7, which were identified in the 35S U5 snRNP described here were absent from the previous preparations. These minor differences are likely due to the use of different antibodies during immunoaffinity chromatography of the 35S U5 snRNPs. **A.** Gallery of 5 selected particle views of the 35S U5 snRNP. The upper row shows band-pass filtered images of individual particles, and the second row shows the corresponding class averages, i.e. cluster centers in an MSA-based unsupervised image clustering. Upon Euler angle determination, row 3 shows the 3D structure under the same view as the two-dimensional projection views in row 2, and row 4 shows computed re-projections from the 3D structure, which are in excellent agreement with the class averages in row 2. The scale bars correspond to 10 nm. **B.** Resolution of the refined cryo-EM map of the 35S U5 snRNP determined from unstained cryo-EM images. The Fourier-Shell-Correlation (FSC) of the cryo-EM map of the 35S U5 snRNP suggests a resolution of 2.42–2.78 nm, depending on the criteria used (i.e. 5σ, 0.143 FSC, 0.5 FSC). **C.** 3D structure of the post-spliceosomal 35S U5 snRNP. The 35S U5 snRNP has a size of ~26.5 nm × 26 nm × 23 nm with maximum dimensions of ~28.5 nm (diagonal as indicated by the arrowheads). The domain numbering (i.e. domains 1, 2b and 3 – 5) is as in Fig. 7.

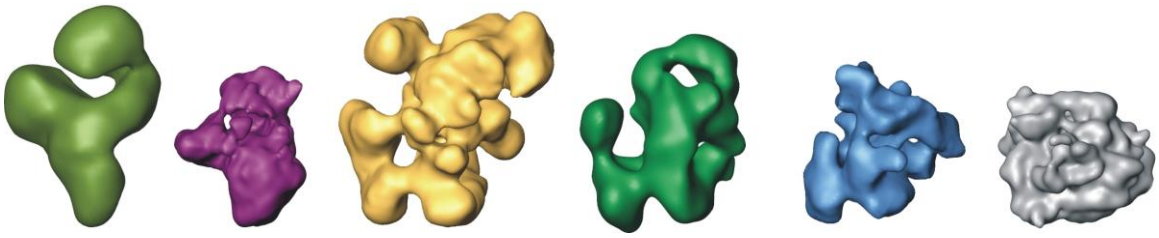

Figure S4. Comparison of the 3D Structures of Human Spliceosomal Complexes and the 70S Ribosome, Related to Figure 7

Shown are the 3D structures of the pre-catalytic BΔU1 complex (EMDB entry 1066; Boehringer et al., 2004), the C complex isolated under stringent conditions (EMDB entry 1062; Jurica et al., 2004), our catalytically active step I spliceosome (C complex) isolated under physiological conditions, our salt-stable RNP core of the C complex, our post-spliceosomal 35S U5 snRNP and the bacterial 70S ribosome (PDB entries 2WRI, 2WRJ, 2WRK, 2WRL; Gao et al., 2009) filtered to slightly better than 3 nm resolution. The structures of the BΔU1 complex and of the C complex isolated under stringent conditions are shown in their (unfitted) standard views as given in the original publications.

Table S1. Details of the Electron Microscopic Data Sets Used for Image Processing, Related to Figure 2

Complex	Type of Imaging	Particle Numbers	Used for
PM5 step I spliceosome (NS)	Negative staining	4,618	2D image processing: class averaging, difference mapping
Salt-stable RNP core of the spliceosome (NS)	Negative staining	29,382	2D image processing: class averaging, difference mapping
Salt-stable RNP core of the spliceosome (Tilt pairs)	Negative staining	63,045 (zero tilt) 6,331 (tilt pairs)	3D image processing: determination of a weighted average RCT structure and 3D class averages
35S U5 snRNP (NS)	Negative staining	59,380	2D image processing: class averaging, difference mapping
$MINX_{GG}$ step I spliceosome (Cryo)	Unstained cryo in vitrified ice	56,202	2D image processing: class averaging
PM5 step I spliceosome (Cryo tilt pairs)	Unstained cryo tilt pairs in vitrified ice	18,152	3D image processing: determination of a weighted average RCT structure
35S U5 snRNP (Cryo tilt pairs)	Unstained cryo tilt pairs in vitrified ice	7,890	3D image processing: determination of a weighted average RCT structure
PM5 step I spliceosome (Cryo refine)	Unstained cryo in vitrified ice	36,071	3D image processing: refinement
35S U5 snRNP (Cryo refine)	Unstained cryo in vitrified ice	21,476	3D image processing: refinement
Anti-MBP labeled C complexes (label at 5' end of 5' exon)	Negative staining	~300 (60 typical views)	2D analysis: Localization of 5' exon end

Supplemental References

Boehringer, D., Makarov, E.M., Sander, B., Makarova, O.V., Kastner, B., Lührmann, R., and Stark, H. (2004). Three-dimensional structure of a pre-catalytic human spliceosomal complex B. Nat Struct Mol Biol *11*, 463-468.

Gao, Y.G., Selmer, M., Dunham, C.M., Weixlbaumer, A., Kelley, A.C., and Ramakrishnan, V. (2009). The structure of the ribosome with elongation factor G trapped in the posttranslocational state. Science *326*, 694.

Jurica, M.S., Sousa, D., Moore, M.J., and Grigorieff, N. (2004). Three-dimensional structure of C complex spliceosomes by electron microscopy. Nat Struct Mol Biol *11*, 265-269.

Makarov, E.M., Makarova, O.V., Urlaub, H., Gentzel, M., Will, C.L., Wilm, M., and Lührmann, R. (2002). Small nuclear ribonucleoprotein remodeling during catalytic activation of the spliceosome. Science *298*, 2205-2208.